Effect of organic modification of sepiolite for PA6 polymer/organoclay nanocomposites

David García-López, José Francisco Fernández, Juan Carlos Merino, Julio Santarén, José María Pastor

PII: S0266-3538(10)00204-6
DOI: 10.1016/j.compscitech.2010.05.020
Reference: CSTE 4725

To appear in: *Composites Science and Technology*

Received Date: 17 December 2009
Revised Date: 10 May 2010
Accepted Date: 23 May 2010

Please cite this article as: García-López, D., Fernández, J.F., Merino, J.C., Santarén, J., Pastor, J.M., Effect of organic modification of sepiolite for PA6 polymer/organoclay nanocomposites, *Composites Science and Technology* (2010), doi: 10.1016/j.compscitech.2010.05.020

EFFECT OF ORGANIC MODIFICATION OF SEPIOLITE FOR PA6 POLYMER/ORGANOCLAY NANOCOMPOSITES

David García-López[1,*], José Francisco Fernández[2], Juan Carlos Merino[1,3], Julio Santarén[4], José María Pastor[1,3]

[1] Center for Automotive Research and Development (CIDAUT), Technological Park of Boecillo, 47151 Valladolid, Spain

[2] Electroceramic Department, Instituto de Cerámica y Vidrio, CSIC. Kelsen 5, 28049 Madrid, Spain

[3] Dpto. Física de la Materia Condensada, E.T.S.I.I. Universidad de Valladolid, 47011 Valladolid, Spain

[4] Grupo TOLSA S.A., Apdo. 38.017, 28080 Madrid, Spain

e-mail: garlop@cidaut.es; Tel.: + 34 983 54 80 35; Fax: + 34 983 14 82 01

ABSTRACT

Polyamide 6 nanocomposites based on sepiolite needle-like clay were prepared via melt extrusion. Sepiolite was organomodified with trimethyl hydrogenated tallow quaternary ammonium (3MTH) by using different amounts of modifier respect to the sepiolite. The effect of modifier/sepiolite ratio on the final nanocomposite properties and the catalytic effect of the sepiolite on the polymeric matrix were evaluated. The presence of organomodified sepiolite on the polymer matrix favoured the crystallinity of the PA6. The catalytic effect of the sepiolite was reduced as the modifier amount increased. The Elastic modulus and Heat Deflection Temperature (HDT) in PA6/organosepiolite nanocomposites increased ~2.5 times respect to the neat PA6 matrix. The higher the modification grade the better the dispersion and orientation of needle-like sepiolite clay were attained. This effect supported the reinforcement efficiency of organosepiolites with high modifier content.

KEYWORDS

Nanocomposite (A), Nanoclay (A), Thermomechanical properties (B), Extrusion (E)

INTRODUCTION

Polymer/clay nanocomposites are a new kind of material with remarkably improved mechanical and physical properties when compared either to the neat polymers or to conventional micro- and macro-composite materials. In fact, higher elastic modulus, barrier properties, flame retardant, high temperature durability are typical features of polymer nanocomposites [1, 2].

The fundamental concept of nanocomposites is based on the high aspect ratios and large interfaces provided by the nanofillers and hence a substantial reinforcement achieved at small loadings. In recent years, various nanoparticles have been used to improve the performance of polymers, including spherical silica [3, 4], layered silicates [5, 6], fibrous silicates [7-8], carbon nanotubes [9], as well synergetic effect between them [10]. The interaction between the primary particles of fibrous silicates is weaker than in the case of layered silicates [11]; consequently a better dispersion can be obtained on polymer nanocomposites and a higher improvement of the mechanical properties can be expected.

Sepiolite is a natural fibrous clay mineral with a typical molecular formula of $Si_{12}O_{30}Mg_8(OH)_4(H_2O)_4.8H_2O$. Sepiolite structure is composed of blocks of two tetrahedral silica sheets sandwiching an octahedral sheet of magnesium oxide hydroxide. The blocks are not sheets but ribbons which are linked forming an open channel similar to that of zeolites. This unique needle-like structure with interior channels (0,36 nm x 1,1 nm) allows a limited penetration of organic and inorganic cations. Due to the discontinuity of the external silica sheet, a significant number of silanol (Si-OH) groups are present at the surface of the sepiolite [12].

The dispersion/defibrillation of the sepiolite in the polyamide 6 matrix and the interfacial adhesion between inorganic/organic components are the main factors to

enhance the nanocomposite properties [5]. Dispersion/defibrillation here means that the contact between sepiolite nanofibres decreases and thus the inorganic/organic interactions maximized. The dispersion degree of the sepiolite must play a key role in the final properties of polymer/organoclays nanocomposites. Recently Bilotti et al. [8] calculated in PA6 the theoretical reinforcement of fibre-like against platelet-like nanoparticles. For a 5% vol of inorganic nanoparticles the elastic modulus of the nanocomposite, E_c, increased respect to the Elastic Modulus of the polymer matrix, E_m, and it is expected to reach a ratio E_c/E_m ~4.2 if both needle or platelet like nanoparticles are unidirectionally oriented. For randomly oriented nanoparticles the E_c/E_m ratio decreased to ~2.4 and ~1.7 for platelet like and fibre-like nanoparticles respectively. Experimental results shown that 2.7% vol of needle-like sepiolite in PA6 produced a lower E_c/E_m ratio ~1.6 than expected. This lower ratio could be in principle attributed to lack of inorganic/organic compatibility or to a poor dispersion. In order to improve the dispersion degree and the compatibility of the nanofiller with the polymer matrix, the sepiolite surface must be modified and appropriated processing must be required.

The structure of the sepiolite presents three sorption/modification sites: (a) oxygen ions on tetrahedral sheets, (b) a small amount of cation-exchange sites, and (c) Si-OH groups along the fibre axis. Adsorption is also influenced by the size, shape, and polarity of the molecules involved. Neither large molecules nor those of low polarity can penetrate the channels, though they can be adsorbed on the external surface, which accounts for 40-50 % of the total specific surface area [13]. Specific organic modifier can be introduced onto the sepiolite based on the surface reactive silanol groups, which it is a fundamental difference between sepiolite and laminar silicates as montmorillonite.

The modification degree of clay could affect both the inorganic/organic compatibility and the dispersion of the sepiolite in the polymer matrix. The purpose of the present

study is to analyze the effect sepiolite modification in the mechanical properties of the nanocomposites.

EXPERIMENTAL SECTION

Sample preparation

The materials used for the preparation of the nanocomposites were commercial PA6 (Akulon F 130-C, DSM). The sepiolite clay was the product Pangel S9 (TOLSA S.A.) with a cation exchange capacity (CEC) of 30 meq/100 g. Modification of the sepiolite was made with a protonated quaternary ammonium salt, specifically trimethyl hydrogenated tallow quaternary ammonium, 3MTH, supplied by Kao Corporation S.A. Different levels of modification with a CEC modifier/sepiolite ratio of 1 (30 meq/100 g), 1.33 (40 meq/100 g) and 1.66 (50 meq/100 g) have been studied and named herein 3MTH-30, 3MTH-40 and 3MTH-50 respectively.

Polyamide 6 nanocomposites containing 6% wt organosepiolite were fabricated via a melt-compounding approach. Both components were mixed in a corrotating twin-screw extruder (Leistritz 27 GL) with barrel temperature between 240 and 250 ºC and 200 rpm of screw speeds. PA6 granulates and organosepiolites were dried prior to blending in the extruder in a vacuum oven for 24 h at 80 ºC in order to remove moisture. To study the best processing conditions the mechanical properties of the nanocomposites obtained with different screw speed were studied, and the product processed at 200 rpm present the best results [14]. The neat PA6 was submitted to identical processing to ensure the same thermomechanical history.

The extrudated material was pelletized and injection moulded into test standard dumbbell-shaped tensile and HDT specimens by using an injection moulding machine

(Margarite JSW110) after being dried at 80 ºC for 24 hours. The temperature of the cylinders was 240–250 ºC and the mould temperature was 80 ºC.

Characterization

The resulting sepiolite organoclays and the obtained nanocomposites were characterized by Thermogravimetric Analysis (TGA, Mettler-Toledo 851e) in nitrogen atmosphere to determine the amount of modifier in the sepiolite as well its degradation temperature. TGA was also used to determine the clay percentage in processed nanocomposites. Differential Scanning Calorimeter (DSC, Mettler Toledo DSC 821/400) and all the processed nanocomposites were performed on small discs of about 10 mg of sample under a nitrogen atmosphere, at 20°C/min as heating and cooling rates. The temperature scans ranged from 25 to 280°C, and backwards. The heat of crystallization for 100 % crystalline PA 6 was taken as 190 J/g [21]. The presence of the PA 6 structural phases in nanocomposites were analyzed by Wide Angle X-ray Diffraction (WAXD, Philips X'Pert MPD with Cu Kα radiation). WAXD scans were performed on the injection-moulded tensile bars with 5º to 50º 2θ range.

The nanostructure of nanocomposites and the dispersion of sepiolite were attempted by Field Emission Scanning Electron Microscopy (FESEM Hitachi H-7000) and Transmission Electron Microscopy (TEM JEOL 2000FX). FESEM analysis was performed on sepiolite organoclays after gold metallization. Before observation the sample was maintained at 60 ºC for 12 hours. TEM analyses were performed on previously dispersed sepiolite organoclays that were deposited in a 200 mesh copper Holey carbon grid and then dried before observation. Nanocomposites in form of 100 nm microtome sections obtained with a Reichert-Jung Ultracut E microtome were also analyzed by TEM. The samples were taken from the middle of the tensile bar. Ultrathin sections around 100 nm in thickness were cryogenically cut with a diamond knife from

the central part of the injection-moulded bars, parallel to the flow direction and 1 mm depth from the surface, in liquid nitrogen environment.

The mechanical properties of the nanocomposite samples were tested using a universal testing machine MTS, model 831-59 according to UNE-EN ISO 527-1. A crosshead speed of 1 mm/min and a dynamic extensometer was used to accurately determine Young´s modulus. Heat deflection temperature (HDT) was measured in a HDT-VICAT tester microprocessor (CEAST 6911.000) according to UNE-EN ISO 75-1 using 1.8 MPa load. All the samples were previously dried in an oven at 80 ºC for 24 h.

RESULTS AND DISCUSSION

Organosepiolites

The Thermogravimetric (TG) and derivate thermogravimetric (DTG) curves of sepiolite without modifier and organosepiolites were shown in Figure 1. Different weight losses were detected. Data were summarized in Table I. The DTG revealed that the burn out of the modifier predominated in addition of the sepiolite weight losses. The first weight loss near 100 ºC was ascribed to water physically bonded to sepiolite on the external surface and in the structural channels [15]. A slight decreasing of this physically bonded water was observed with the modifier content. This fact indicates a more hydrophobic nature of the surface. However, the high specific surface area of the organosepiolite always retained water and organoclays required an oven drying before compounding. This first weight loss was previously reported by Dusquesne et al. [15] but other authors omitted their presence by using thermogravimetric curves starting from 150 ºC [16-17]. The second weight loss region ranged from ~180 ºC to 400 ºC mainly related to the modifier decomposition. Pristine sepiolite lossed at ~ 300 ºC two of the four crystallization water molecules. The elimination of the other two molecules occurred at

525 ºC. The DTG showed the removal velocity of these water molecules in the organosepiolites. Meanwhile the low temperature removal of crystallization water overlapped with the modifier elimination, the high temperature ones seemed quite similar in the different organosepiolites. Grafted sepiolite with aminopropoxyl groups increased the low temperature elimination of the 2 water molecules [15], but there was not available information related to the effect of surfactant adsorption thorough the sepiolite-surface hydroxyl groups. When the modifier content was equal to the CEC of the sepiolite a single weight loss peak with a maximum at 355 ºC was observed. This peak was slightly asymmetric with a tail at higher temperature that could be related to modifier incorporated at interfibre sites or into the zeolitic channels of the sepiolite. If the modifier exceeded the sepiolite CEC, the maximum of such peak occurred at lower temperatures and its asymmetry enhanced. This fact indicated that modifier excess adsorbed onto the modifier bonded to the sepiolite. Modifier exceeding the CEC of the sepiolite, which is not interacting directly with the sepiolite, was evidenced by the presence in DTG of a decomposition peak at ~240ºC The presence of free modifier that not interacted with sepiolite surface could be detrimental for melt compounding of the PA6 nanocomposites because the processing temperature was 240–250 ºC. The final step of the sepiolite weight losses corresponded to the removal of constitution water or hydroxyl groups around 750 ºC [18] and occurred in organosepiolites at lower temperature than in pristine sepiolite. This temperature reduction could be originated by the modifier residues

FESEM micrographs showed the fibrous morphology of pristine and modified sepiolite, Figure 2. The interactions between nanofibres formed dense 10-30 μm in size aggregates for the pristine sepiolite. The modification process produced a reduction in size of aggregates that showed flake type morphology. The weakening of the aggregates

after organic modification was independent of the sepiolite/modifier ratio (not shown on behalf of their similarity) and therefore mainly attributed to the organoclay processing. Moreover, many single fibres can be observed clearly in both samples but most of the fibres retain a strong interaction between them after the modification process.

TEM micrographs showed the pristine sepiolite fibres having needle morphology of ~30-50 nm in diameter and ~1-5 μm in length, Figure 3a. These fibres formed bundles-like aggregates by surface interaction between individual needle-type particles. Large fibres were observed but there were formed by connected fibres as confirmed by detailed observation of disperse single sepiolite fibres. The modified sepiolite presented also needle morphology but nanofibres became more dispersed, Figure 3b. The modified sepiolites showed similar diameter and reduced length to 300-1000 nm. The surface interaction between individual needle-type particles was also reduced. The presence of modifier in excess was confirmed by the appearance of a secondary phase irregular in shape, cloud type which was circle-marked for shake of clarity in Figure 3c. The aspect ratio of the modified sepiolites ranged in the interval of 30-200 in agreement with the aspect ratio observed by Bilotti et al [8].

Nanocomposites

The TG and DTG of the PA6/organosepiolite nanocomposites showed a single peak with a maximum of the weight loss velocity, T_{max}=470 ºC for the pure PA6, Figure 4. The presence of organosepiolite in PA6 matrix has shifted T_{max} 5 ºC (T_{max}= 465 ºC) in all nanocomposites compared with the value obtained in PA6. Tartaglione et al. found [17] that the T_{max} in PP/sepiolite nanocomposites was reduced by the presence of the sepiolite but the maximum weight velocity increased considerably related to the catalytic site effect in the inner part of the zeolitic pores in agreement with previous studies [19]. The catalytic action of the sepiolite was considerably reduced when

sepiolite was modified by mercaptosilane grafting [17]. By the contrary the incorporation of octyltrimethoxysilane modified sepiolite in low density polyethylene stabilized the thermal decomposition by formation of a protective surface layer [16]. The present study revealed that in PA6/sepiolite nanocomposites the catalytic activity of the zeolitic channel was reduced probably because these zeolitic channels or the inter-nanofibre space of aggregates were partially filled by the 3MTH modifier, thus an excess of modifier was slightly more effective to reduce the catalytic activity of the nanosepiolite in PA6 nanocomposites. However differences in the matrix stability and in the degree of sepiolite dispersion must be considerer to elucidate this mechanism.

DSC heating and cooling curves of the nanocomposites showed the effect modifier/sepiolite ratio on the crystallization behaviour, Figure 5. The melting temperature (Tm), the crystallization temperature (Tc), ΔHc, and corresponding crystallinity (Xc) are presented in Table II. The crystallinity values were calculated on second melting scans following the procedure previously described [20]. During heating scan the presence of the organoclay introduced relatively slight differences that consisted in a reduction of the temperature for the low temperature peak with the modifier/sepiolite ratio meanwhile the maximum temperature slightly reduced for all the nanocomposites in comparison with the PA6. During cooling scans the Tc increased for all the nanocomposites indicating that the sepiolite acted as a nucleating agent for the crystallization of polyamide. Bilotti et al. [7] showed a larger increase of the Tc for polypropylene reinforced with sepiolite and proposed a second mechanism to reduce the nucleating efficiency based on the lack of dispersion for sepiolite nanofibres. The increasing of Tc was also reported by Xie et al. [21] in PA6 but without changes in the crystallinity. The sample PA6-3MTH-50 shown clearly two melting peaks at 215ºC and 226 ºC corresponding to crystalline γ and α polyamide phases respectively. These peaks

were also present in all nanocomposites as the asymmetry of the observed peak showed [22]. The area of the melting peak at 215ºC increased with increasing content of modifier on the sepiolite indicating an increasing amount of the γ-phase present in the nanocomposites. However, the degree of crystallinity of the nanocomposite polymer decreased slightly with increasing amount of modifier used for the preparation of the organosepiolite. The presence of the modifier on the sepiolite surface seems thus to limit the nucleating efficiency of the nanoparticles acting as an interphase.

The phase composition of the PA6 nanocomposites was also obtained by profile analysis of the WAXD scans as illustrated in Figure 6. The peak at 7.2º 2θ corresponds with the (100) crystal plane of the sepiolite and it was the only peak of the sepiolite that possessed relevance in the nanocomposites. This peak increased in intensity that could be associated with the preferential orientation of sepiolite nanofibres during the injection. Moreover this peak slightly displaced to lower 2θ when compared with pristine sepiolite that could be related to and expansion effect favored by the bounded polymer due differences in thermal expansion coefficient between the inorganic particles and the organic matrix. The WAXD patterns showed the coexistence of polyamide α-phase and γ-phase. The peak at 21.2º 2θ was assigned to the (002) crystal plane of γ-phase. Two peaks at 20º and 23.5º 2θ were assigned respectively to the (200) and (002) crystal planes to the α-phase [23-24]. The neat polyamide shown mainly crystalline α-phase and the nanocomposites showed increasing of γ-phase. The increasing of γ-phase in PA6/montmorillonite nanocomposites have been reported previously [25-26]. In the present study the excess of modifier does not affect markedly the crystalline phases that were quite similar for the different nanocomposites. The nanocomposite should also exhibit a preferential orientation and γ-phase that it is expected to grow on the montmorillonite sheets. By the contrary the here studied neat

polyamide shown low presence of α-phase. Although crystallinity was not increased with the presence of sepiolite these particles acted as nucleation sites to grow more perfect crystals. The x-ray diffraction diagram shows an intense and broader peak at 25.7º 2θ assigned to a combination of different polyamide α crystalline peak, (010) (110) and (210) [27-28]. The appearance of theses crystalline peaks have been reported in sepiolite/PA6 nanocomposites nor in montmorillonite/PA6 nanocomposites due probably to less confinement effect of fibrous particles against layered ones [20].

Figure 7 shown TEM micrographs of nanocomposites. The nanofibres in Figure 7a showed a randomly orientation with contact between them forming bundles aggregates with lengths of 100-300 nm. Evidence of non-aligned fibres along the injection direction was observed by the presence of grey circles on the top of fibres corresponding to the local heating during microtome sample preparation in spite of the nitrogen cooling. The Figure 7b and 7c showed fibres with higher lengths of 300-800 nm. The aspect ratio range of the sepiolite in the different nanocomposites slightly decreased but it kept in values of ≈100-200 nm. This fact indicated the shortening of nanofibres during the processing by breaking or by separation of connected nanofibres in the apparent large sepiolite fibres. The randomly oriented nanofibres seems to have a lower aspect ratio due in part to nanofibres cutting during ultracut microtome processing as evidence by the presence of grey circles.. Higher modifier/sepiolite degree with values of 40 and 50 meq/100 g favoured the dispersion/defibrillation behaviour and better alignment of nanofibres during the extrusion of nanocomposites. The nanofibres evolved from in part randomly oriented to unidirectionally oriented as the modifier increased because of the reduction of sepiolite-sepiolite interactions.

Table III summarized mechanical properties values of nanocomposites. The sepiolite percentage in the nanocomposites was evaluated from thermal losses by

thermogravimetric analysis. In all the samples the final percentage of sepiolite was ~6 % wt. For comparison, the elastic modulus and HDT values of the pure PA6 were also listed. It clearly stated that for a similar amount of sepiolite the significant improvement of both the elastic modulus and the HDT correlated with the modifier/sepiolite ratio. Such improvement was based on the dispersion and alignment of the sepiolite nanofibres in the PA6 matrix as discussed above. The presence of modifier at the surface of the nanofibre reduced the catalytic activity of the inorganic phase. In addition the presence of modifier inhibited the nucleating efficiency of the γ-phase that could also contributed to the overall behaviour.

By comparison of the present result with the theoretical predictions of Billoti el al. [8] we have obtained with the addition of ~6 % wt of modified sepiolite in PA6 matrix a E_c/E_m ratio ~2.5, meanwhile the maximum expected ratio was ~4.2 for unidirectionally oriented nanofibres and ~1.7 for randomly ones. Billoti et al [8] only found a E_c/E_m ratio of 1.6 for unmodified sepiolite. These results shown clearly that the organomodification improved the defibrillation and alignment of nanofibres.

Both the Elastic modulus and the HDT can be reinforced in PA6/clays nanocomposites. Previous works of PA6/montmorillonite nanocomposites for allowed obtaining a HDT_c/HDT_m ratio ~2 when nanoclays where modified with octadecylamine (MMT-ODA) [6] and a ratio of ~1.8 when modified montmorillonite with 3MTH [29]. All these result have been enhanced in the present work with ratio up to ~2.6 by using the organomodified sepiolite indicating that. In spite of the higher aspect ratio of layered clays the organomodified sepiolite were more effective in the reinforcement of the PA6 polymer matrix.

CONCLUSIONS

The PA 6 nanocomposites based on sepiolite have shown different morphologies and properties according to the ratio of sepiolite/modifier. The presence of modifier on the sepiolite reduced their catalytic activity on the polymer matrix increasing the Tc of the PA6 and also acted as a nucleating agent for the crystallization of the mainly γ-phase of PA6. Nanocomposites with the highest amount of modifier reached the best mechanical properties as well as the greatest dispersion grade.

The mechanical properties obtained present E_c/E_m ratio up 2.5 that was also similar for the HDT properties. These improvements were higher than those achieved in PA 6 nanocomposites if compared with layered nanoclays in spite of their lower aspect ratio. The reduction of the sepiolite-sepiolite interactions by the modifier favoured the better dispersion and alignment of nanofibres that were translated to effectiveness in the reinforcement mechanism.

ACKNOWLEDGMENTS

This work is supported by CICYT MAT2007-66845-C02-01 and MAT2008-06379-C02, and the Consejería de Educación of the Junta de Castilla y León (GR104).

REFERENCES

1.- Zanetti M, Lomakin S, Camino G. *Polymer Layered Silicate Nanocomposites*. Macromol Mater Eng 2000; 279: 1-9.

2.- Paul DR, Robeson LM. *Polymer nanotechnology: nanocomposites*. Polymer 49 2008; 49: 3187–3204.

3.- Yang ZZ, Qiu D, Li J. *Waterborne dispersions of a polymer-encapsulated inorganic particle nanocomposite by phase-inversion emulsification*. Macromol Rapid Comm 2002; 23: 479-483.

4.- Crivello JV, Mao Z. *Preparation and Cationic Photopolymerization of Organic-Inorganic Hybrid Matrixes*. Chem Mater 1997; 9: 1562-1569.

5.- Pinnavaia TJ, Beall GW. "*Polymer-clay nanocomposites".* Wiley. New York, 2000.

6.- García-López D, Gobernado-Mitre I, Fernández JF, Merino JC, Pastor JM. *Influence of clay modification process in PA 6-layered silicate nanocomposite properties*. Polymer 2005; 46: 2758-2765.

7.- Bilotti E, Fischer HR, Peijs T. *Polymer nanocomposites based on needle-like sepiolite clays: Effect of functionalized polymers on the dispersion of nanofiller, crystallinity, and mechanical properties*. J Appl Polym Sci 2006; 107: 1116-1123.

8.- Bilotti E, Zhang R, Deng H, Quero F, Fischer HR, Peijs T. *Sepiolite needle-like clay for PA6 nanocomposites: An alternative to layered silicates?* Comp. Sci. Tech. 2009; 69: 2587-2595.

9.- Baughman RH, Zakhidov AA, de Heer WA. *Carbon Nanotubes – The Route Towards Applications*. Science 2002; 297: 787-792.

10.- Cardenas M, García-López D, García-Vilchez A, Fernández JF, Merino JC, Pastor JM. *Synergy between organo-bentonite and nanofillers for polymer based fire retardant applications*. Appl Clay Sci 2009; 45: 139-146.

11.- Lu H, Seng H, Song Z, Shing K, Tao W, Nutt S. *Rod-Like Silicate-Epoxy Nanocomposites*. Macromol Rapid Commun 2005; 26: 1445-1450.

12.- Grim R. E. *Clay mineralogy*. McGraw-Hill. New York, 1962.

13.- Galan E. Properties and applications of palygorskite-sepiolite clays. *Clay Miner* 1996; 31*:* 443-453.

14.- 7º Congreso Nacional de Materiales compuestos (MATCOMP07). *Estudio de las condiciones de proceso para la obtención de materiales nanocompuestos de PA 6 basados en sepiolitas*. 2007.

15.- Dusquesne E, Moins S, Alexandre M, Dubois P. *How can Nanohybrids enhance polyester sepiolite nanocomposites properties?*. Macromol Chem Phys 2007; 208: 2542-2550.

16.- García N, Hoyos M, Guzmán J, Tiemblo P. *Comparing the effect of nanofiller as thermal stabilizers in low density polyethylene*. Polym Degrad Stab 2009; 94: 39-48.

17.- Tartaglione G, Tabuani D, Camino G, Moisio M. *PP and PBT composites filled with sepiolite: Morphology and thermal behaviour*. Compos Sci Technol 2008; 68: 451-160.

18.- Singer A, Galan E. *Palygorskite-Sepiolite ocurrente, Genesis and Use*. Elsevier. Amsterdam, 1984.

19.- Marcilla A, Gomez A, Menargues S, Ruiz R. *Pyrolysis of polymers in the presence of a commercial clay*. Polym Degrad Stab 2005; 88: 456-460.

20.-. Xie S, Zhang S, Liu H, Chen G, Feng M, Qin H, Wang F, Yang M. *Effects of processing history and annealing on polymorphic structure of nylon-6/montmorillonite nanocomposites*. Polymer 2005; 46: 5417-5427.

21.- Xie S, Zhang S, Wang F, Yang M, Seguela R, Lebebvre JM. *Preparation, structure and thermomechanical properties of nylon-6/nanocomposites with lamella-type and fiber-type sepiolite*. Compos Sci Technol 2007; 67: 2334-2341.

22.- Medellín-Rodríguez F, Larios-López JL, Zapata-Espinoza A, Dávalos-Montoya O, Phillips PJ, Lin JS. *Melting Behavior of Polymorphics: Molecular Weight Dependence and Steplike Mechanisms in Nylon-6*. Macromolecules 2004; 37: 1799-1809.

23.- Kohan MI. *Nylon Plastics Handbook*. Hanser Publishers, 1995.

24.- Murthy N.S., Curran S.A., Aharoni S.M. and Minor H., *Premelting crystalline relaxations and phase-transitions in Nylon-6 and 6,6.* Macromolecules, 1991; 24:3215-3220.

25.- Varlot K., Reynaud E., Kloppfer M. H., Vigier G. and Varlet J. *Clay-Reinforced Polyamide: Preferential Orientation of the Montmorillonite Sheets and the Polyamide Crystalline Lamellae*. J. Polym. Sci. B Polym. Phys. 2001; 39:1360–1370.

26.- Liu T., Tjiu W. C., He C., Na S. S. and Cheng T. S. *A processing-induced clay dispersion and its effect on the structure and properties of polyamide 6*. Polym. Int. 2004; 53:392–399.

27.- Lin S.Y., Chen E. C., Liu K. Y., Wu T. M. *Isothermal Crystallization Behaviour of Polyamide 6,6/Multiwalled Carbon Nanotube Nanocomposites*. Polym. Eng. Sci. 2009; 49: 2447–2453.

28.- Ricou P., Pinel E., Juhasz N. *Temperature experiment for improved accuracy in the calculation of Polyamide-11 crystallinity by X-Ray Diffraction*. Pp. 170-175 in JCPDS - International Centre for Diffraction Data 2005, Advances in X-ray Analysis, Volume 48.

395 29.- Fornes TD, Yoona PJ, Hunterb DL, Keskkulaa H,. Paul DR. *Effect of organoclay*
396 *structure on nylon 6 nanocomposite morphology and properties*. Polymer 2002; 43:
397 5915-5933.
398

399 **TABLE CAPTIONS**

400 Table I. Thermogravimetric analysis values of pristine sepiolite and sepiolite modified

401 with 3MTH.

402 Table II. Crystallization data of samples from DSC scans.

403 Table III. Mechanical properties of PA 6 nanocomposites.

404

405

406 **FIGURE CAPTIONS**

407

408 Figure 1. (a) Thermogravimetric and (b) DTG curves for the controlled rate analysis of
409 pristine sepiolite and sepiolite modified with 3MTH.

410 Figure 2. SEM images of pristine sepiolite (a) and modified sepiolite (b).

411 Figure 3. TEM images of pristine sepiolite (a) and modified sepiolite (b) 3MTH-30 and
412 (c) 3MTH-50, the circle-marked areas shown the presence of excess of modifier.

413 Figure 4. TG-DTG of PA 6 and its nanocomposites.

414 Figure 5. DSC first heating (a), cooling (b) and second heating (c) scans of PA 6 and its
415 nanocomposites. The curves are vertically offset for clarity.

416 Figure 6. WAXD of sepiolite without modifier, PA 6 and its nanocomposites.

417 Figure 7. TEM images of nanocomposites: PA 6-3MTH-30 (a) PA 6-3MTH-40 (b) and
418 PA 6-3MTH-50 (c).

419

Table I. Thermogravimetric analysis values of pristine sepiolite and sepiolite modified with 3MTH.

Organoclay	**25-125 ºC**		**125-450 ºC**		**450-650 ºC**		**650-850 ºC**		**Organic modifier %**
	Mass %	**T (ºC)**	**Mass %**	**T (ºC)**	**Mass %**	**T (ºC)**	**Mass %**	**T (ºC)**	
SEPIOLITE	4.87	77	3.72	280	2.22	524	1.87	793	-
3MTH-30	1.34	71	6.99	340	4.90	528	5.76	733	5.95
3MTH-40	1.41	78	8.72	332	5.96	538	5.58	738	8.74
3MTH-50	0.74	79	2.61 8.61	232 342	6.57	539	5.58	740	11.85

Temperature values were measured on the mid-point of the curve that corresponds to the decomposition of the 50 wt% of the compound

Organic modifier was evaluated between 125-650 ºC

Table II. Crystallization data of samples from DSC scans.

Sample	**Tm (°C)**		**Tc (°C)**	**ΔHm (J/g)**	**Xc (%)**
PA 6	228		178	63.1	33.2
PA 6-3MTH-30	226		180	59.8	33.7
PA 6-3MTH-40	226		180	60.0	33.9
PA 6-3MTH-50	215	226	183	55.7	31.5

Table III. Mechanical properties of the nanocomposites of PA 6.

Sample	Elastic Modulus (MPa)	Variation of the Elastic modulus (%)	HDT (ºC)	Variation of the HDT (%)	% wt Sepiolite TGA
PA 6	2665 ± 180	-	49 ± 0.1	-	-
PA 6-3MTH-30	5483 ± 70	106	96 ± 1	96	5.9
PA 6-3MTH-40	6455 ± 610	142	102 ±6	107	6.1
PA 6-3MTH-50	6385 ± 180	140	129 ± 1	165	6.2

Figure 1

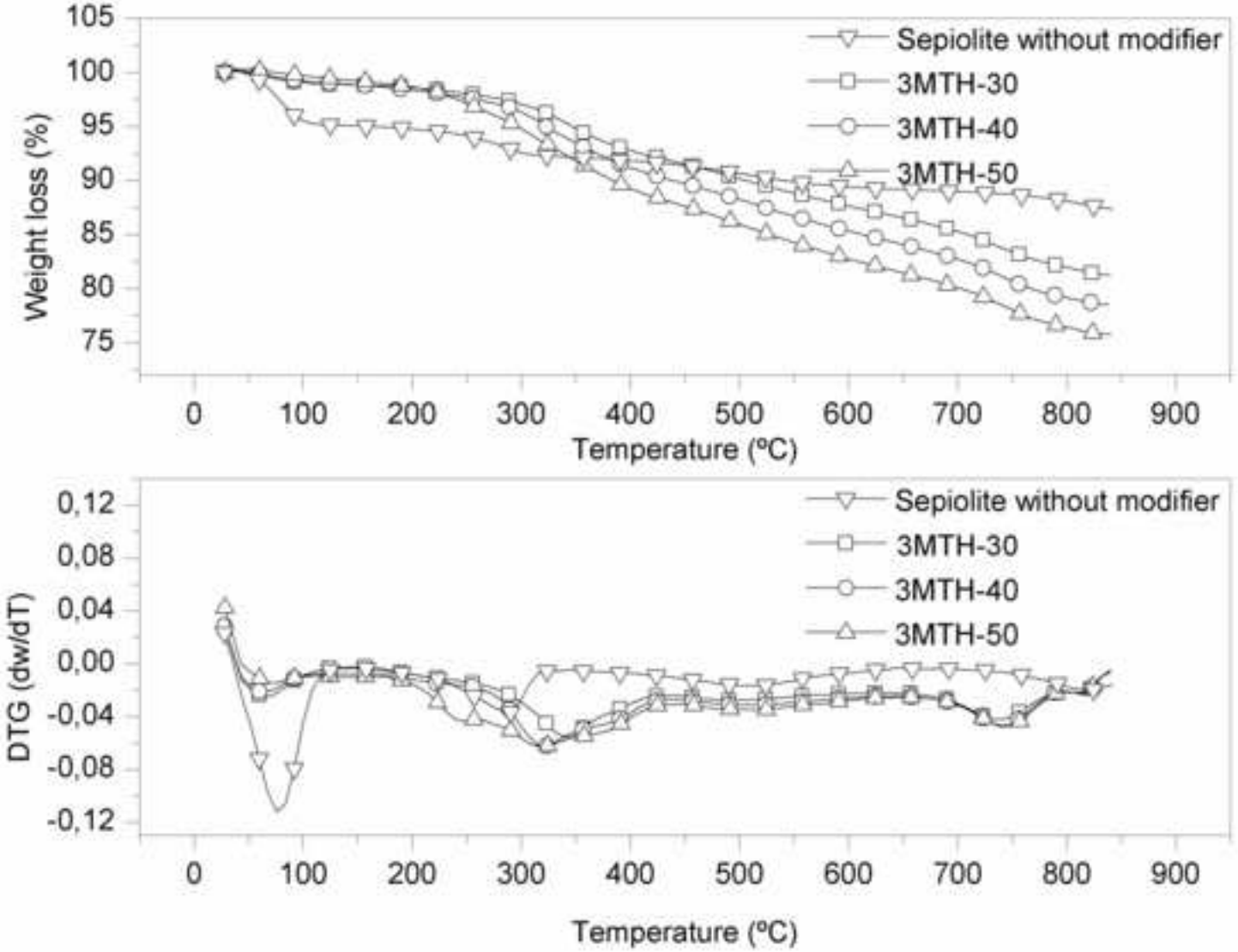

Figure 2a

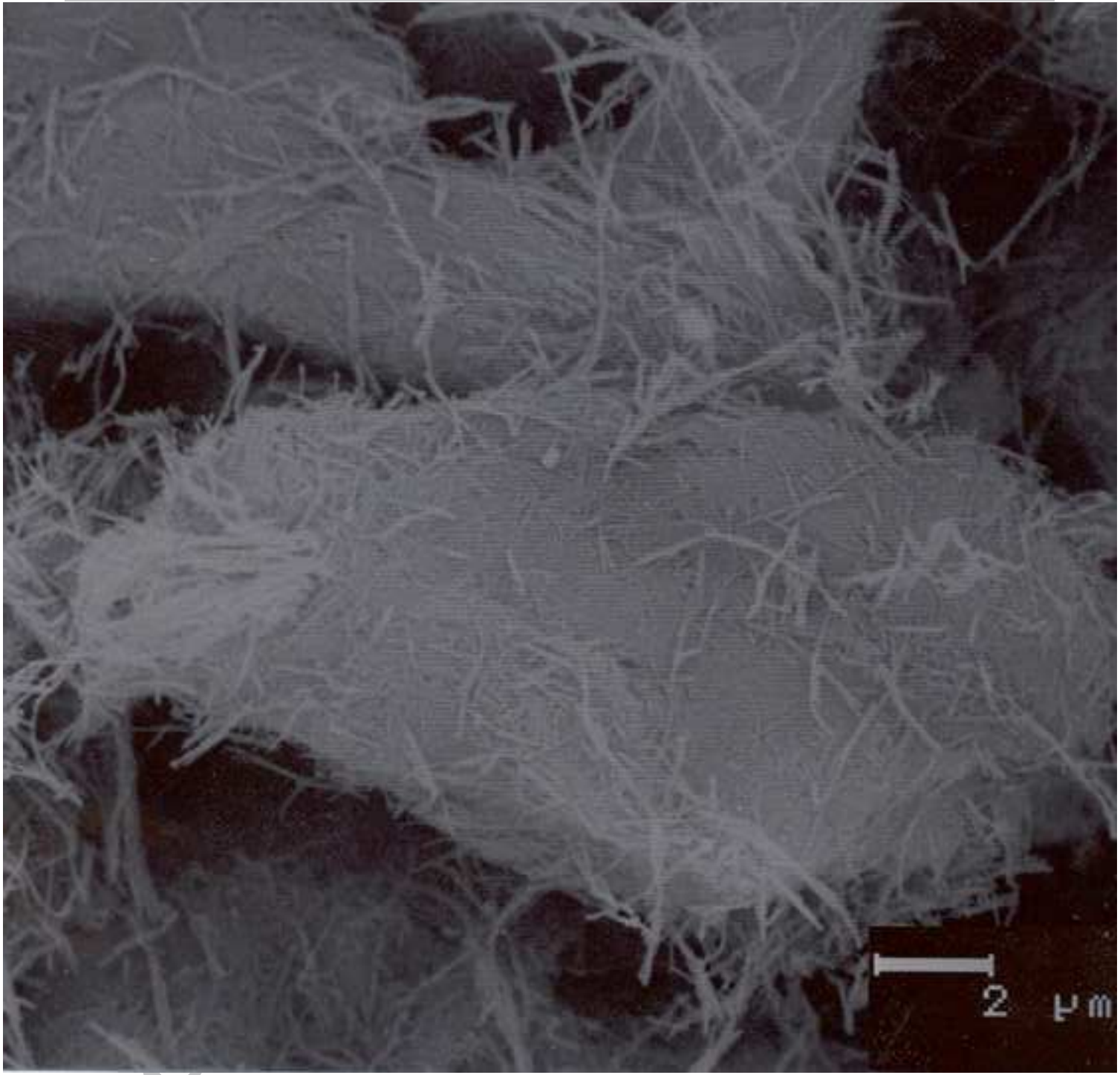

Figure 2b

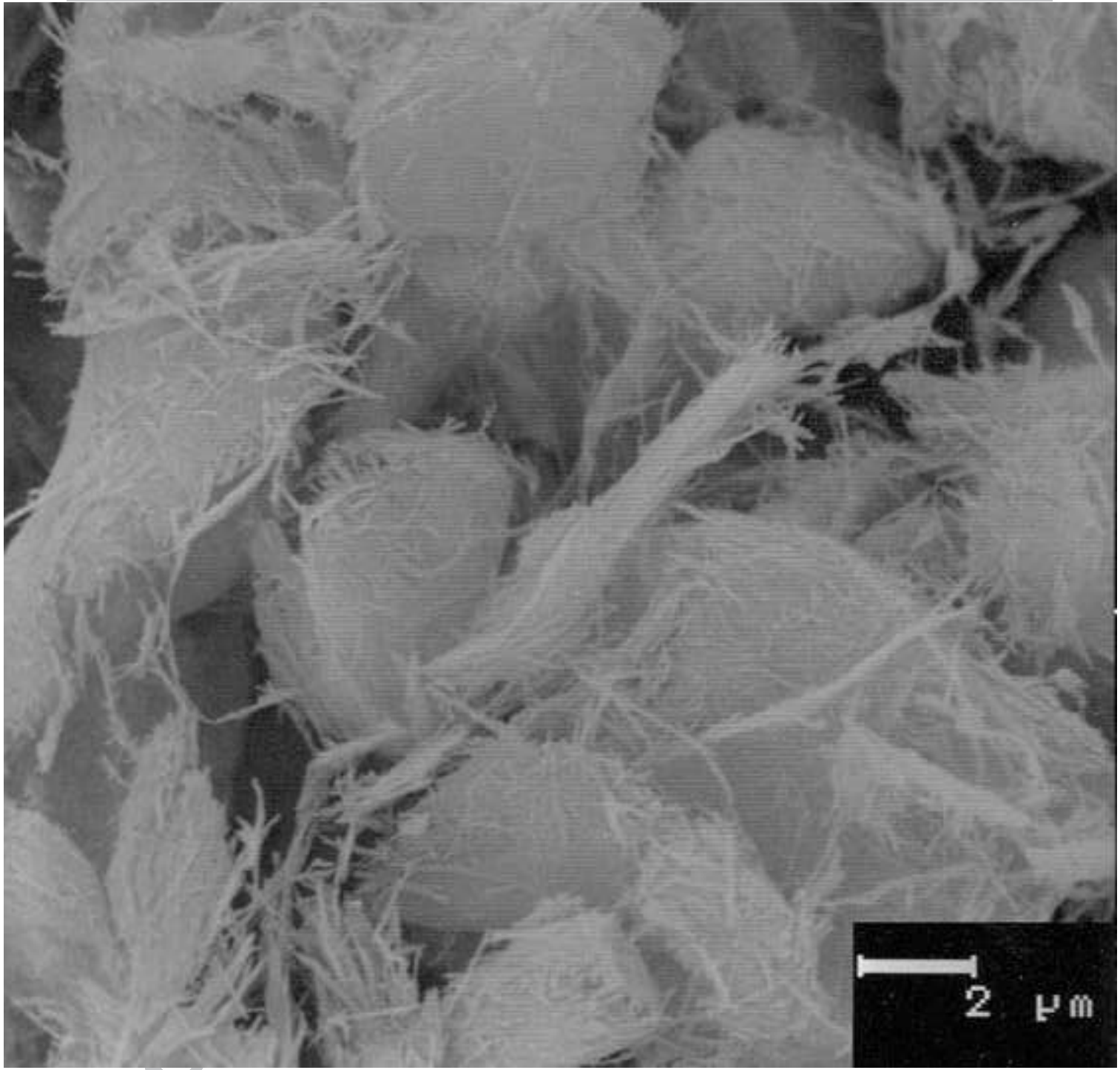

Figure 3a

Figure 3b

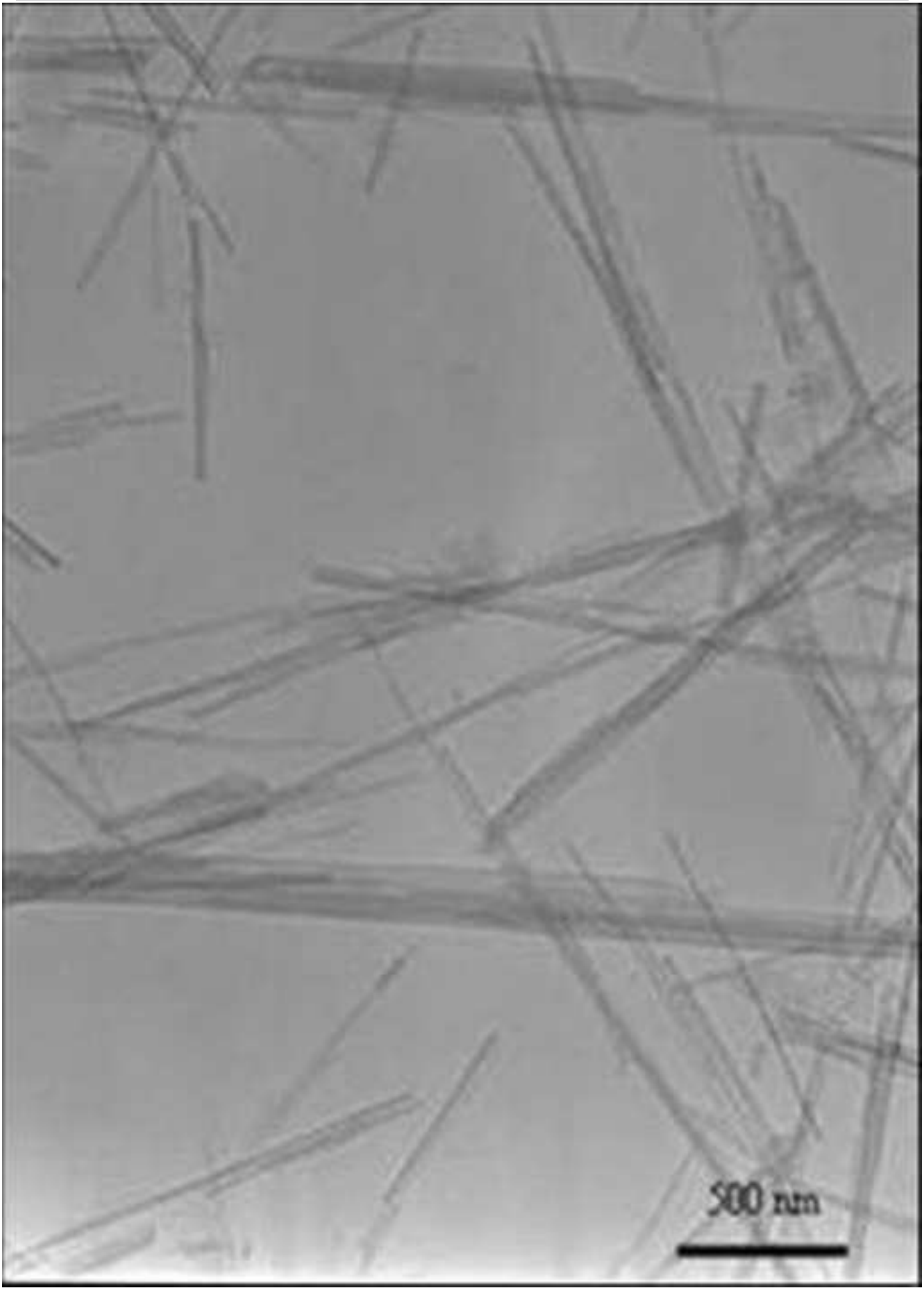

Figure 3c

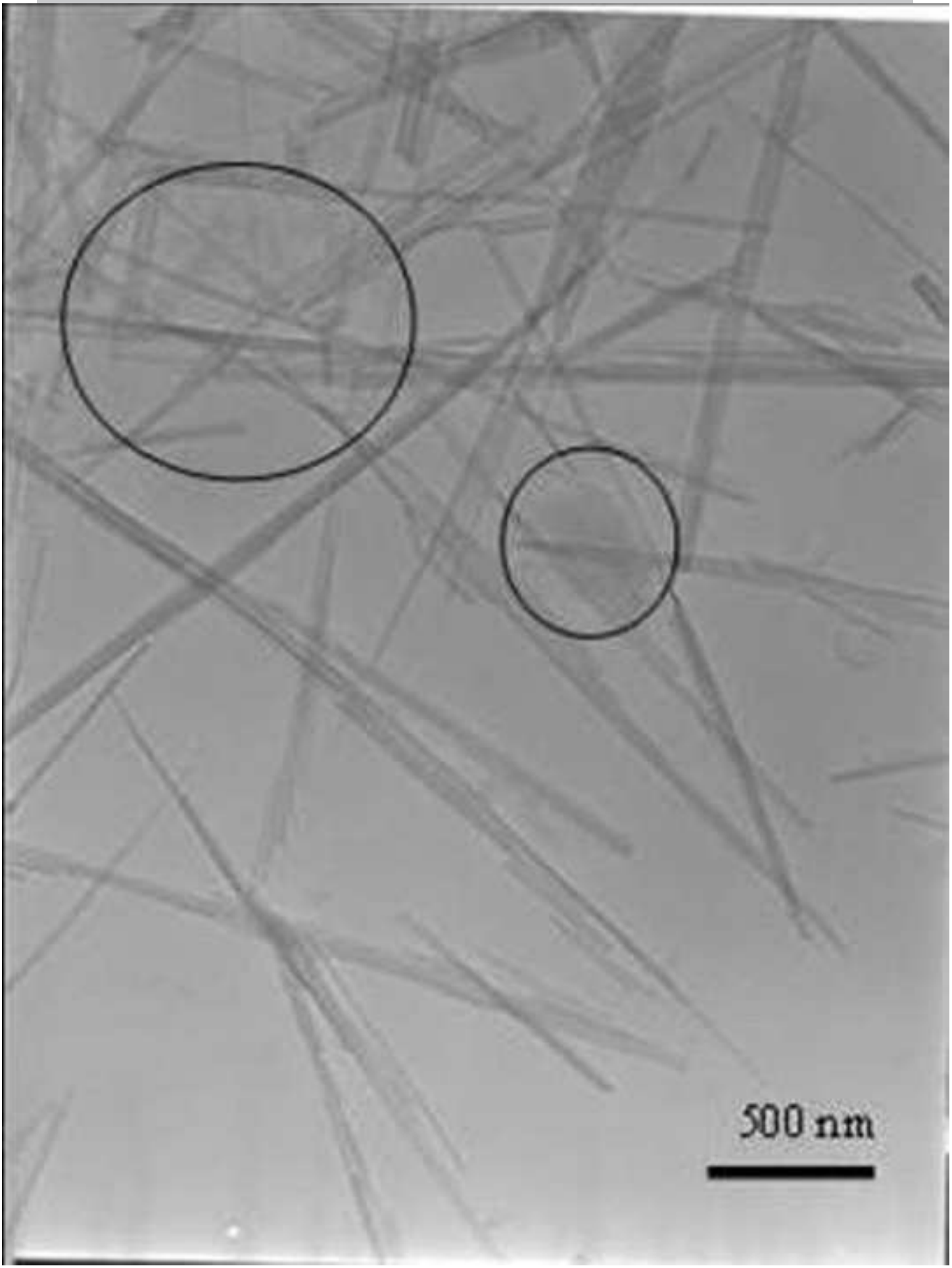

Figure 4

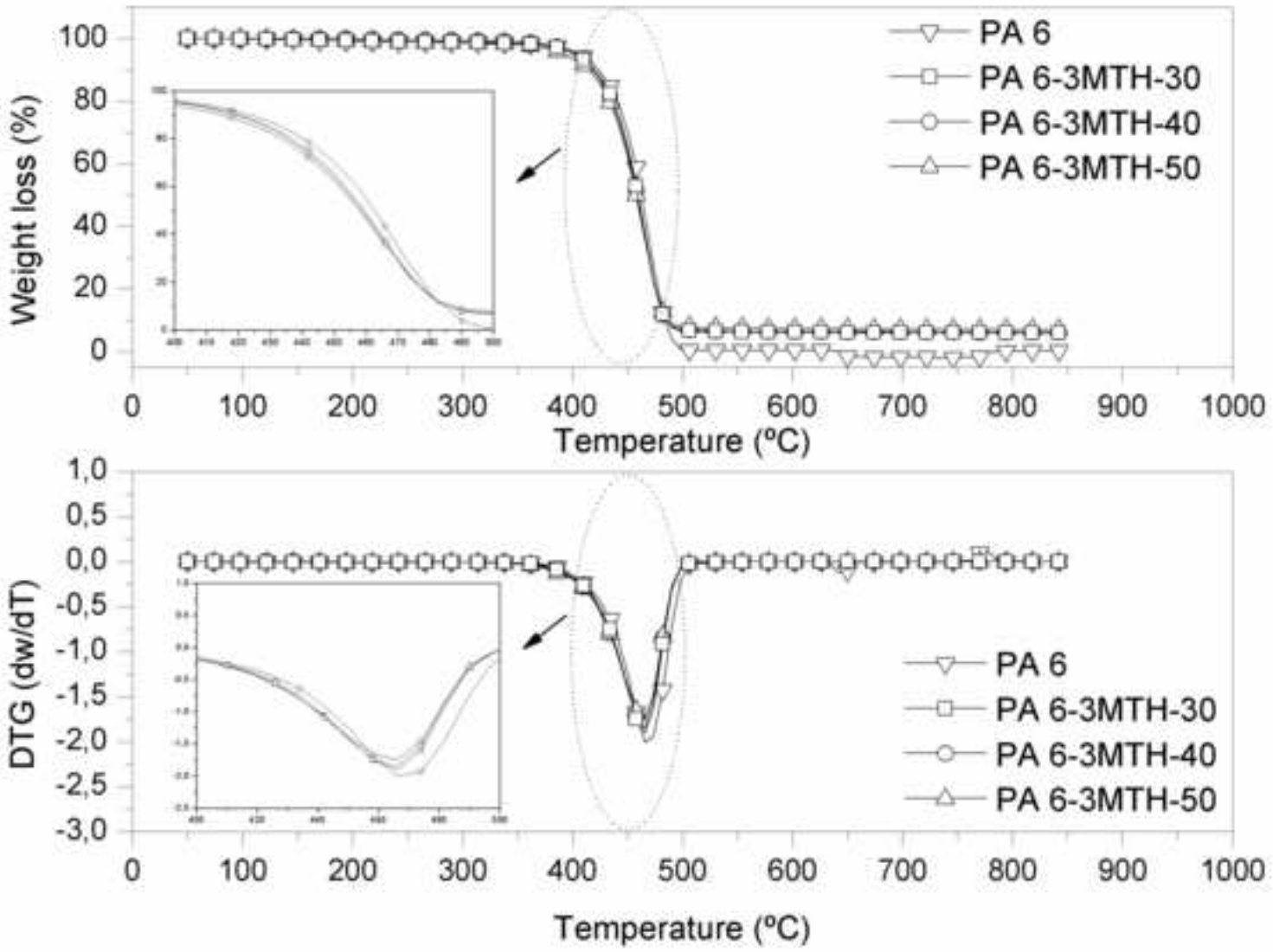

Figure 5a

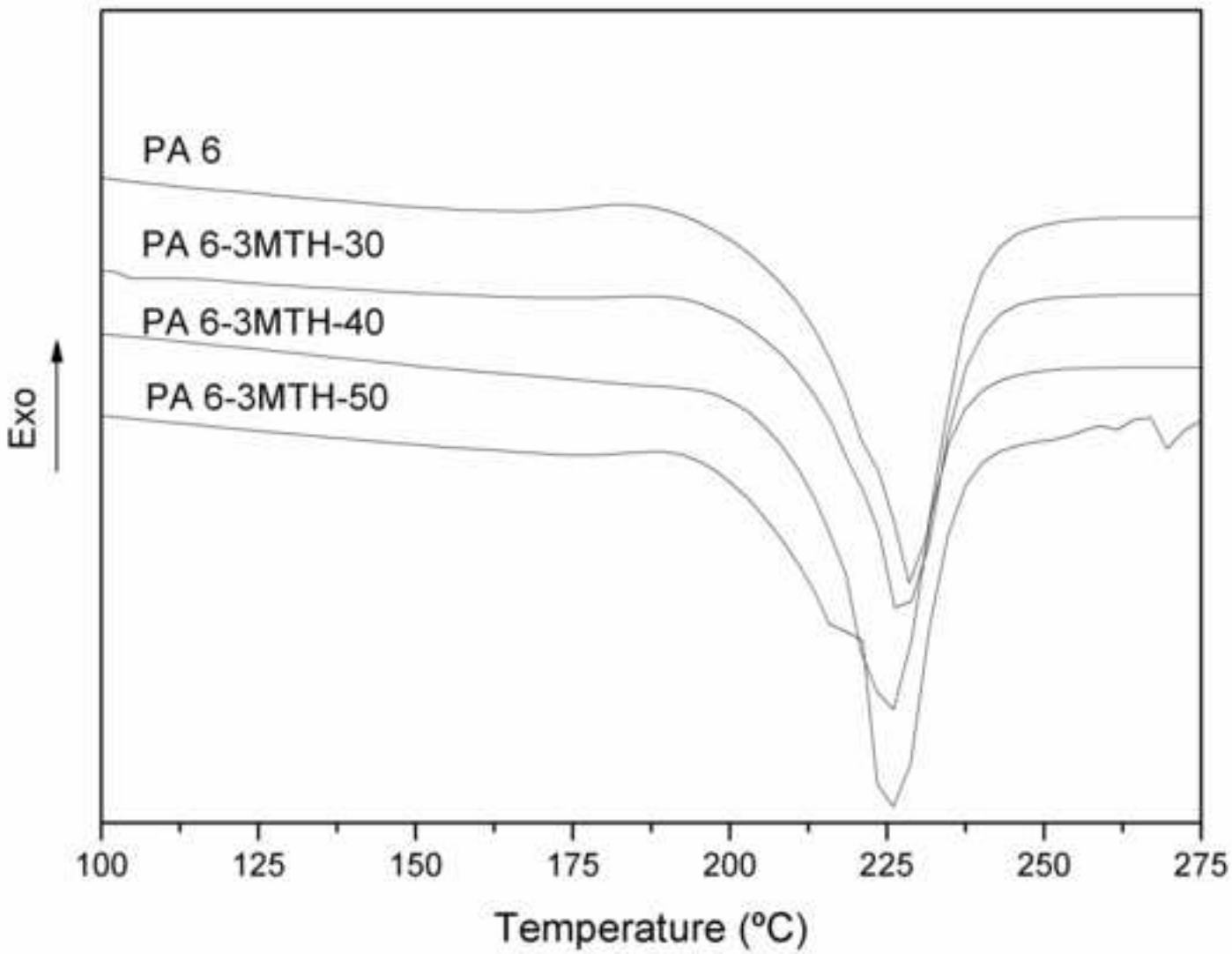

Figure(5b

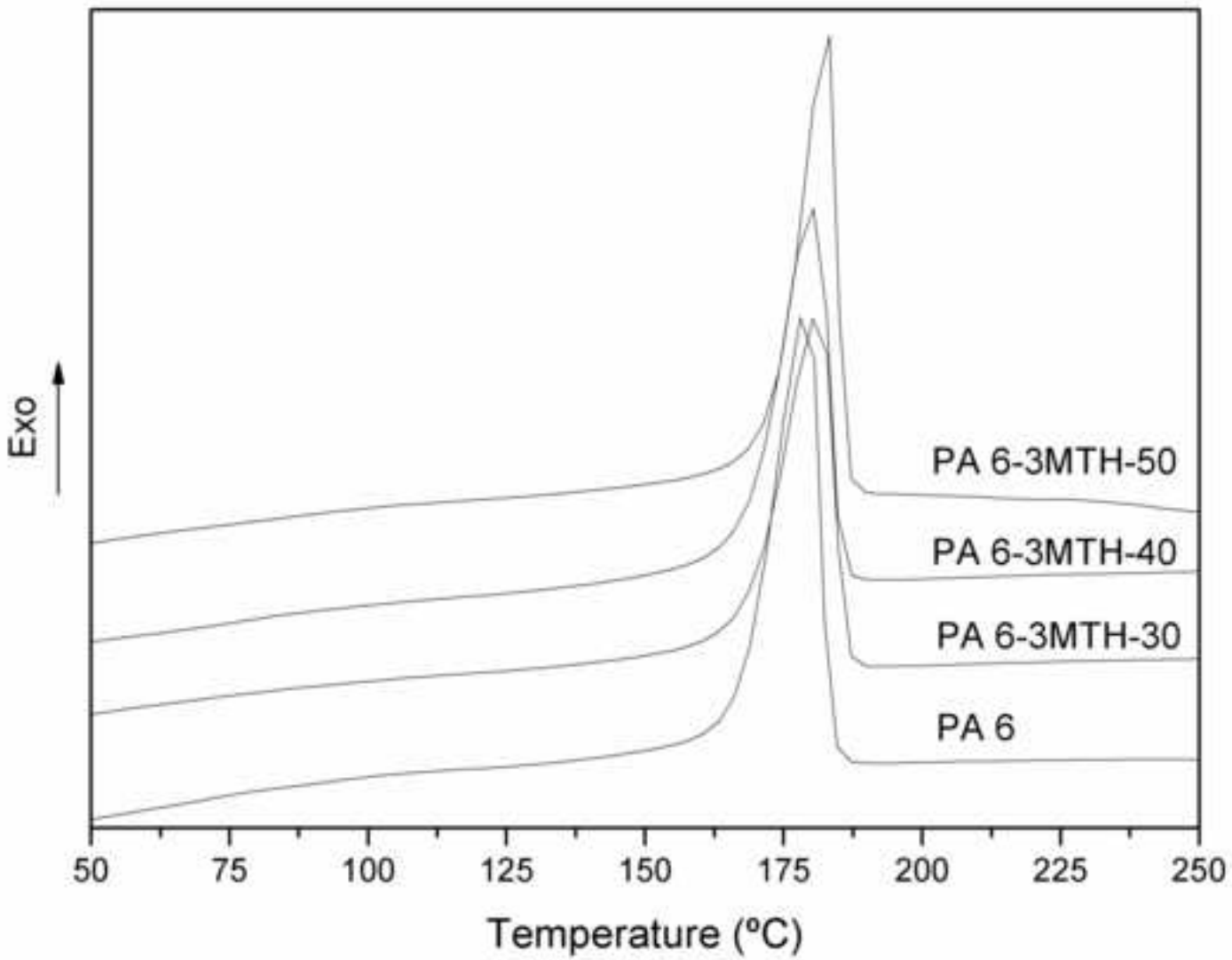

Figure 5c

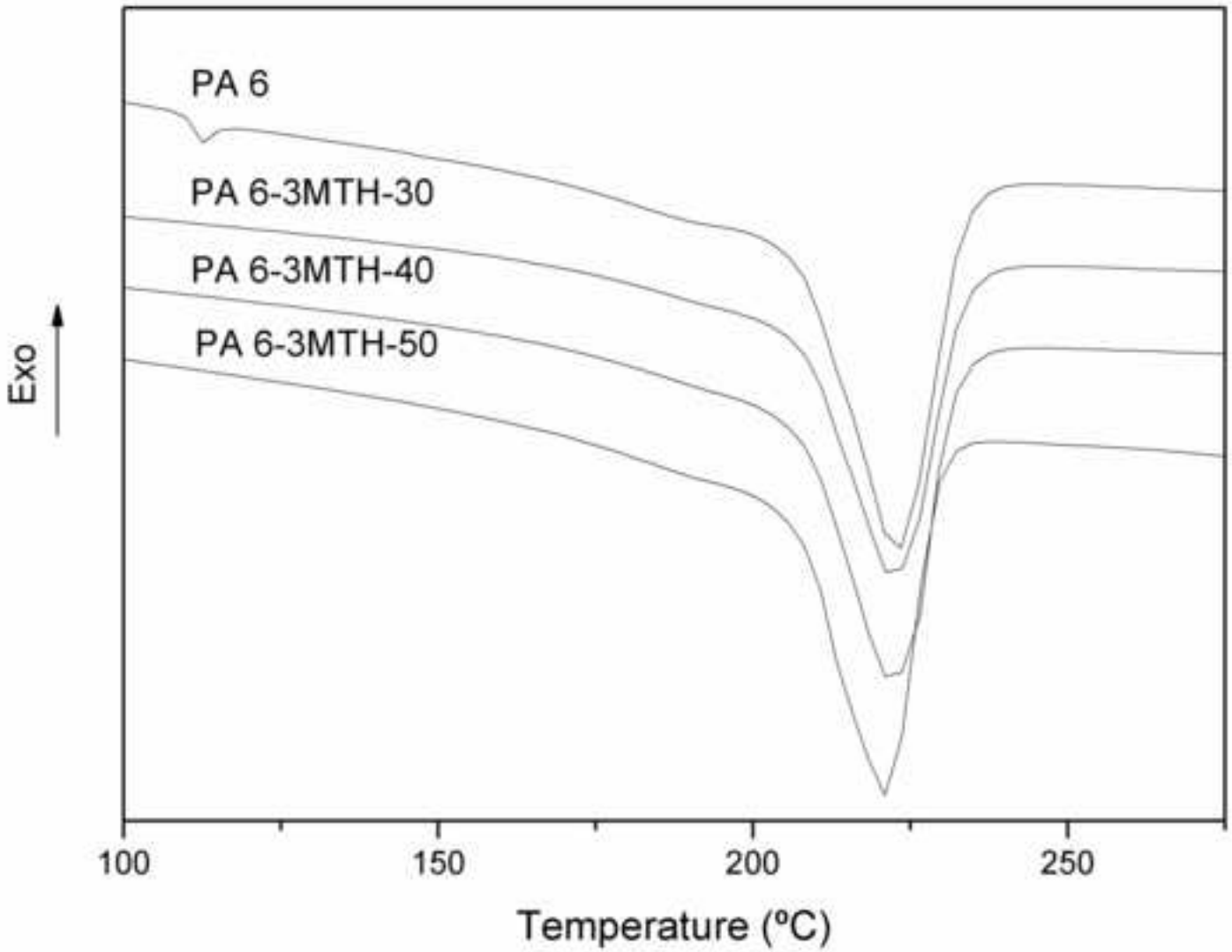

Figure 6

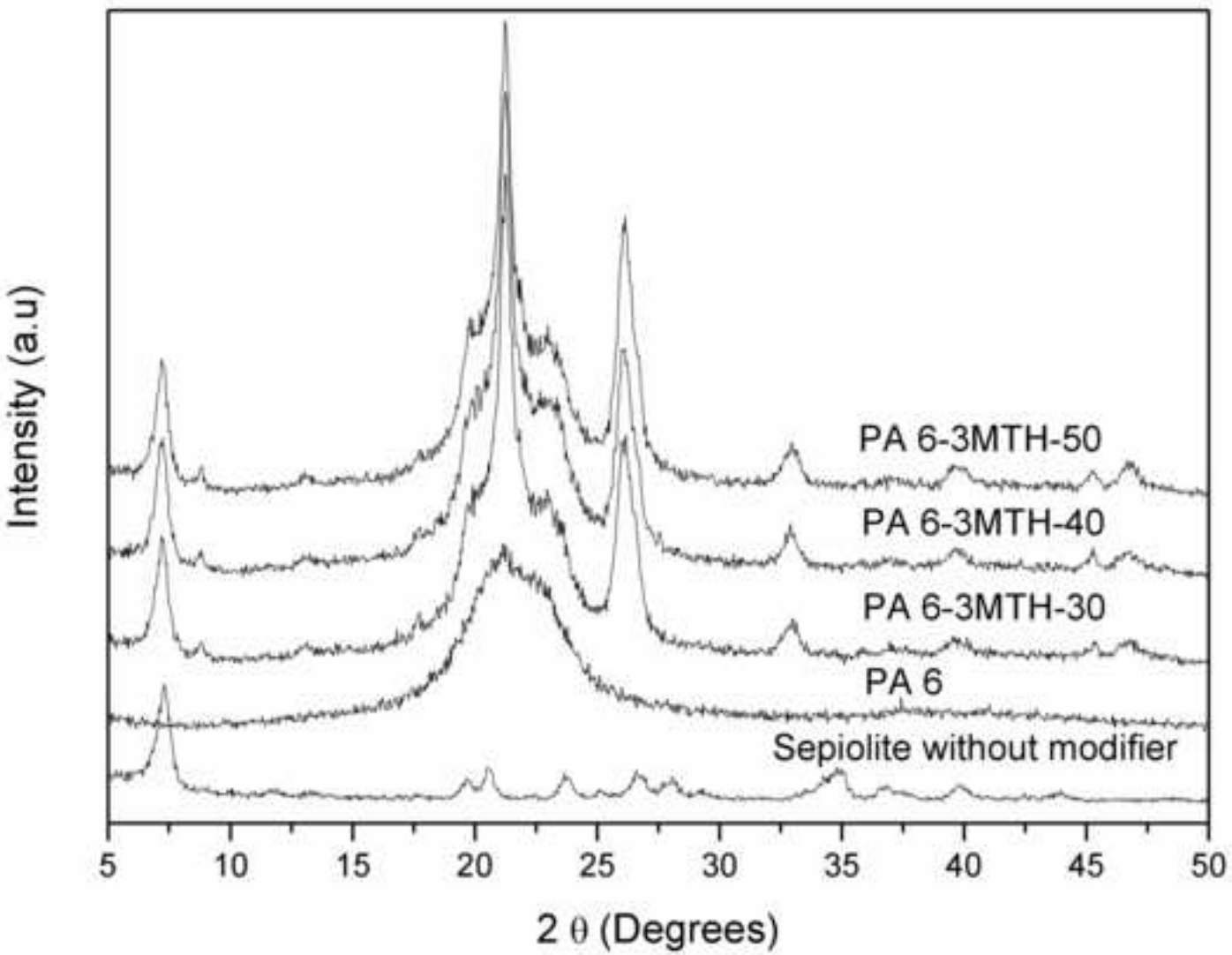

Figure 7a

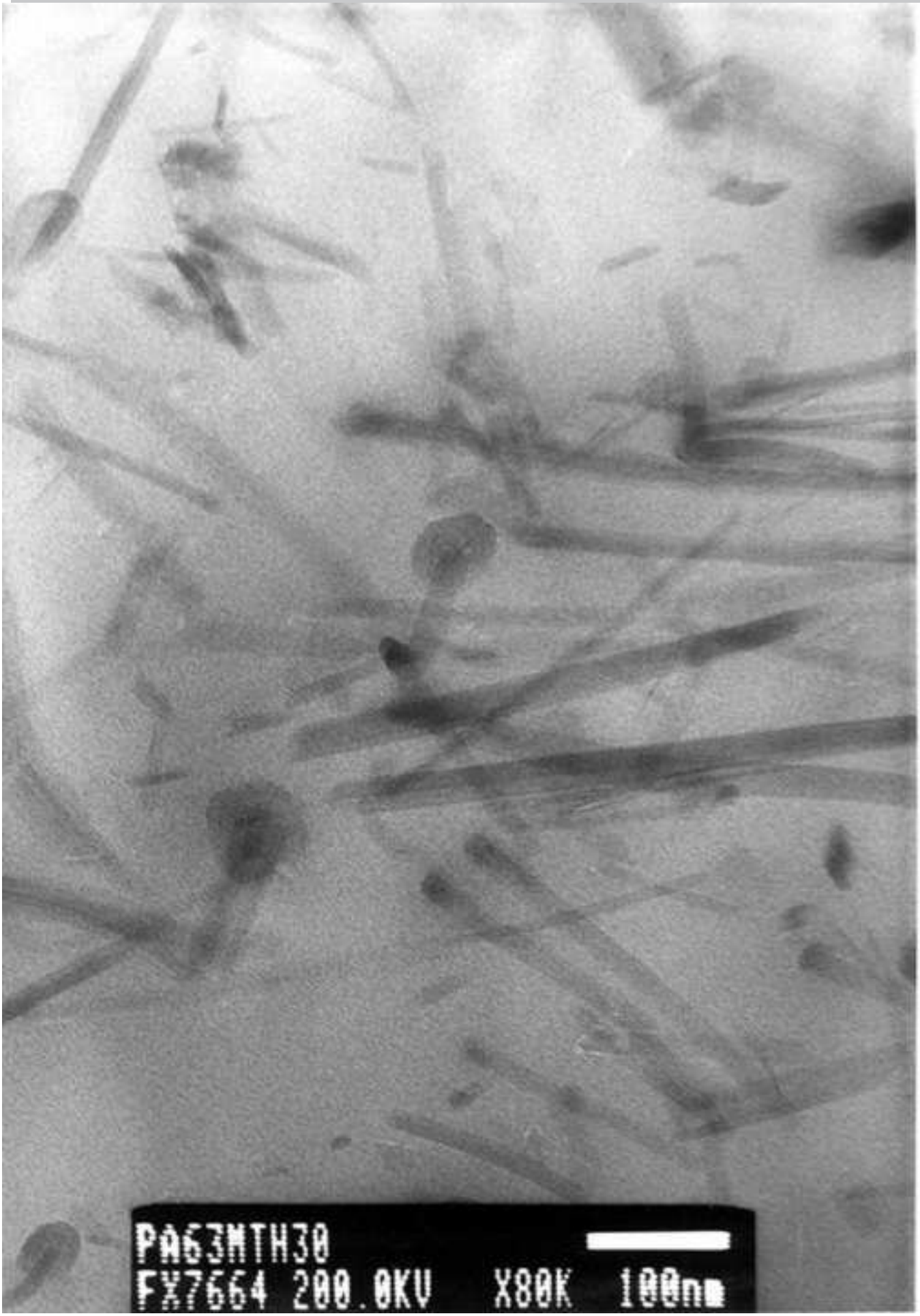

Figure 7b

Figure 7c